Direct observation of the ponderomotive force effects in short-scale-length laser plasmas by frequency-domain interferometry

P. Audebert, J.-P. Geindre, S. Rebibo,* and J.-C. Gauthier
Laboratoire pour l'Utilisation des Lasers Intenses, UMR7605, CNRS-CEA, Université Paris VI, Ecole Polytechnique, 91128 Palaiseau Cedex, France

(Received 14 February 2001; published 29 October 2001)

We report on single-shot frequency-domain interferometric measurements showing space- and time-resolved ponderomotive electron density profile steepening of a short-scale-length ultraintense laser-produced plasma. The density gradient scale length is varied by applying a time-delayed laser prepulse. The measured absolute position of the critical density surface is found to be in agreement with one-dimensional hydrodynamic simulations for the range of scale lengths studied.

DOI: 10.1103/PhysRevE.64.056412 PACS number(s): 52.50.Jm, 52.35.Mw, 52.70.Kz

The continuous development of ultrahigh intensity, short-pulse lasers over the past years and the study of their interactions with plasmas have led to a number of proposed applications such as electron and proton accelerators, coherent generation of short-wavelength radiation, x-ray lasers, and fast ignition of inertial confinement fusion [1]. In most of these applications long laser propagation distances are required, very much greater than the Rayleigh range of usual focusing optics. To overcome this problem, laser channeling of intense laser pulses in plasmas can be produced by a variety of driving forces. At the lower intensities of up to 5×10^{15} W/cm^2, laser-guiding structures have been produced by the thermally driven laser-induced expansion [2] of a preformed plasma and the quasibound mode structures of the resulting plasma waveguide have been analyzed [3]. At the highest laser intensities currently achievable, of above 10^{19} W/cm^2, self-modulation, relativistic self-focusing, and electron density displacement (cavitation) are the principal mechanisms for self-channeling of laser pulses in plasmas [4]. In this regime, thermal forces are overwhelmed by ponderomotive forces dominated by the relativistic quiver motion of the electrons that translates into large light pressure [5,6]. In the intermediate laser intensity regime, a competition between thermal and ponderomotive forces has been observed during the interaction of a subpicosecond laser beam with a flat solid target [7]. In this context, the inward-directed ponderomotive force acting on the electrons is comparable to the force exerted by the thermal pressure gradients responsible for coronal expansion. This regime (laser intensity of 5×10^{17} W/cm^2 and 300 fs pulse duration) was used by Chien *et al.* [8] and Peyrusse *et al.* [9] to confine the thermal expansion and to allow high ''averaged hot density'' plasmas to be produced.

Following the seminal experimental work performed by Liu and Umstadter [7] at laser intensities around 10^{16} W/cm^2, only scarce experiments have been undertaken to explore the ponderomotive laser interaction regime at higher laser intensities, although theory have revealed many of its fascinating aspects. For example, numerical experiments, using particle-in-cell simulations [10] predicted Rayleigh-Taylor-like instabilities of the overdense plasma boundary and the corresponding growth rates were calculated [11]. Of course, the experimental aspect of these studies is difficult because only few optical techniques are available to study the dynamics of expanding electron density profiles from solid-target plasmas. Resonance absorption profile spectroscopy [12], based on the angle and polarization dependence of the absorption of a probe laser is restricted to electron density gradient scale lengths of $kL\approx1$, where k is the laser wave number and L the electron density gradient scale length $L=[(1/n_e)(dn_e/dz)]^{-1}$. Doppler shift spectroscopy of reflected probe pulses has been used successfully at the lower end of the laser intensity range [13,14]. The analysis of the line shift and linewidth of backscattered or reflected fundamental and/or second harmonic radiation has been exploited to study ponderomotive effects in the high-intensity regime [15]. Short-pulse laser plasma accelerations of more than $10^{17}g$ have been observed [16] with such a technique and the wavelength shift of high harmonics [17] has also been exploited to infer plasma dynamics.

Because of the steepness of the electron density gradient in short-pulse laser-produced plasmas ($L/\lambda\ll1$, where λ is the laser wavelength), spectral Doppler spectroscopy techniques measure the velocity of the moving plasma, with temporally varying reflectivity [18]. A more direct estimation of the ponderomotive effects in rapidly expanding plasmas would be to measure directly the position of the critical surface, where the electron density equals the critical density n_c. This can be done by using a phase-sensitive optical technique such as frequency-domain interferometry [19]. This technique has been widely used in ultrafast laser-matter interaction experiments including molecular spectroscopy [20], laser-induced dielectric damage [21], laser wakefield particle acceleration [22], and femtosecond shock waves [23]. In laboratory plasmas, we have successfully exploited this technique to measure the electron density gradient scale length [24], the onset of optical breakdown in dielectric materials [25], the collisionality of ultrafast plasmas [26], and we have extended its applicability to single-shot measurements [27,28]. In this paper, we report on space- and time-resolved measurements of the laser ponderomotive effects in carefully scale-length-controlled short-pulse expanding plasmas. Re-

*Present address: Altran Technologies, Paris, France.

sults are compared with state-of-the-art hydrodynamics simulations incorporating ponderomotive forces calculated from first principles [29]. We show the recess of the critical surface under the influence of the laser light pressure with subpicosecond and 15 μm time and space resolution, respectively.

The experiments were performed using the 100 TW chirped pulse amplification beamline at the Laboratoire d'Utilisation des Lasers Intenses (LULI). Frequency-doubled (laser wavelength of 0.529 μm) laser pulses with up to 10 J and pulse durations of 400 fs were delivered onto target by an $f/8$ off-axis parabola. The targets consisted of optically polished carbon plates and the *S*-polarized laser beam was incident at 60° angle from the target normal. A preformed plasma was deliberately produced on target by a delayed prepulse of the same duration as the main pulse with the help of a Mach-Zehnder interferometer-type delay line located before amplification in the laser chain. The time delay could be varied between 0 and 10 ps. The beam diameter of the prepulse was reduced by a 3 mm diameter aperture to provide a near diffraction-limited focal spot of 90 μm diameter full width at half maximum. The energy ratio between the two pulses was controlled by rotating the laser polarization before the polarization-splitting entrance of the delay line. The original laser polarization, compatible with the direction of dispersion of the compression gratings, was restored after the interferometer by a half-wave plate. The energy contrast between the two overlapping pulses was high enough to avoid any severe nonlinear effects in the laser chain during the final amplification [30].

The time delay between the two pulses was determined with high precision from the fringe spacing recorded in the spectral domain at the output of a spectrometer. Finally, the two pulses were compressed to 400 fs and frequency doubled by a 5 mm thickness potassium dihydrogen phosphate crystal to increase the intensity contrast ratio. The main pulse was slightly defocused to keep small-scale intensity fluctuations larger than the 15 μm effective spatial resolution of the frequency-domain interferometric diagnostic. The intensity distribution obtained at the target plane was made of a 30 μm diameter central peak surrounded by a 150 μm diameter shoulder. The prepulse focal spot size was not affected by this small defocusing due to its small *f* number. An auxiliary beam of a few millijoules energy was taken from the main laser chain and compressed by a different grating-pair compressor to provide a linearly chirped, 24 ps duration, 1.058 μm wavelength, probe pulse. The 27° incidence angle of the probe beam with respect to target normal was chosen so that the electron densities at the turning point of the main beam (10^{21} cm^{-3}) match approximately the electron densities at the turning point of the probe beam. The probe beam diameter, of millimeter size, encompassed largely the main pulse laser-affected zone and the surrounding laser-free target surface. Because of our energy division scheme based on polarization, it was not possible to vary independently the prepulse and the main pulse levels. Accordingly, the prepulse laser irradiance was varied between 5×10^{14} and 2×10^{15} W/cm^2 and the main pulse irradiance was varied between 2.5×10^{17} and 5×10^{17} W/cm^2.

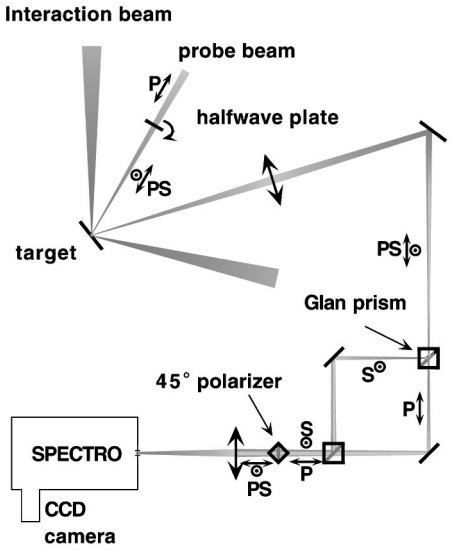

FIG. 1. Experimental setup showing the pump and probe beams configuration, the interferometer, and the combination of the spectrometer and the CCD detector.

The main diagnostic used in this experiment is a dual-quadrature Mach-Zehnder interferometer in which amplitude division is used to obtain spectral information from the reference and the signal in a single shot, simultaneously in *S* polarization and *P* polarization. The principles of dual-quadrature frequency-domain interferometry have been described previously [24]. Figure 1 gives a schematic view of the experimental apparatus. The polarization of the probe beam is rotated by 45° with respect to the plane of incidence with a half-wave plate. After reflection from the target, the probe focal spot is imaged on the entrance polarization separation prism of the Mach-Zehnder. The interferometer is globally set with equal arm path lengths but the beam wave fronts are slightly tilted and shifted so that the plasma-perturbed *P*-polarization component of the probe pulse interferes with the unperturbed *S*-polarization component. The beams are then recombined in a second prism, and their polarization is projected along their bisector to allow the formation of interference fringes. The entrance prism is imaged again on the entrance slit of a 1-m homemade Czerny-Turner spectrometer. A 16-bit charge-coupled-device (CCD) camera records the spectrum. The spatial resolution is limited by the 15 μm fringe spacing measured in the focal plane. A calibration shot, without the main laser and the prepulse beams, is necessary to define the instrumental phase null. More details on the experimental system and of the signal analysis are given elsewhere [28]. To summarize, the complex reflection coefficient $R(\omega)$ and the phase shift $\Delta\Phi(\omega)$ are extracted from the comparison of the signal and reference shots, in a manner similar to the one described in Ref. [19]. With the knowledge of the probe pulse chirp parameter a, which can be easily determined experimentally, the perturbation in time can be recovered. Indeed, the field of the chirped pulse can be written in the frequency domain,

$$\vec{E}_0(\omega)=E_0(\omega)\exp[j(\omega-\omega_0)^2/a]. \quad (1)$$

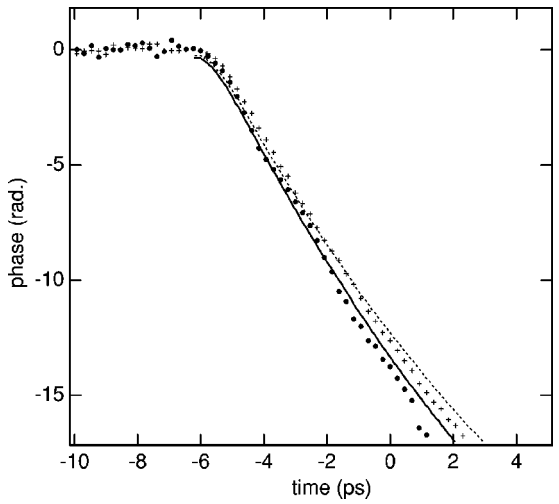

FIG. 2. Phase shift of *P*- and *S*-polarized probe beams as a function of time following the interaction of a pure carbon target with the 400 fs duration LULI laser prepulse. Circles, *S* polarization; crosses, *P* polarization. Hydrocode results for *S* polarization (solid line) and for *P* polarization (dashed line) are shown for comparison. A phase shift of 11.2 rad corresponds to a displacement of the probe pulse turning point of one wavelength (1.0529 μm).

We construct the signal by multiplying the field by the plasma perturbation, so that,

$$\vec{E}(\omega)=\vec{E}_0(\omega)\sqrt{R(\omega)}\exp[j\Delta\Phi(\omega)]. \tag{2}$$

The perturbation $P(t)$ in the time domain can be now easily recovered by using an inverse-Fourier transform,

$$P(t)=\mathcal{F}^{-1}[E(\omega)]/E_0(t), \tag{3}$$

where $E_0(t)$ is the original chirped pulse in the time domain. With this signal reconstruction procedure, based on the knowledge of the chirp parameters, we reach a time resolution comparable to the compressed probe pulse duration.

Figure 2 shows time-resolved measurements of the phase shift of the reflected probe beam in *S*- and *P*-polarization in the case of an interaction with the prepulse beam only at an irradiance of 2×10^{15} W/cm^2. We stress again that these measurements are taken in a single shot. Using the reconstruction procedure described in Ref. [28], the time resolution is comparable to the duration of the compressed probe pulse, i.e., about 500 fs. The small difference between the phase measured in the two polarizations is easily explained when we take into account the electron density gradient and the probe beam incidence angle in the analysis (see Fig. 5 of Ref. [24]). The absolute displacement of the reflected probe turning point is about 1μm in 5 ps. Using the (*P*-*S*) phase difference measured in Fig. 2 and the calibration results of Ref. [24], the electron density gradient scale length at a delay time of 6 ps after the prepulse is $L/\lambda=0.7\pm0.05$ (λ is the wavelength of the probe laser). At a time delay of 3 ps, the reduced gradient scale length is $L/\lambda=0.2\pm0.1$. Experiments have been compared to the predictions of the FILM hydrodynamics code simulations [31] with time-dependent coupled atomic physics for carbon. This code has been modified to

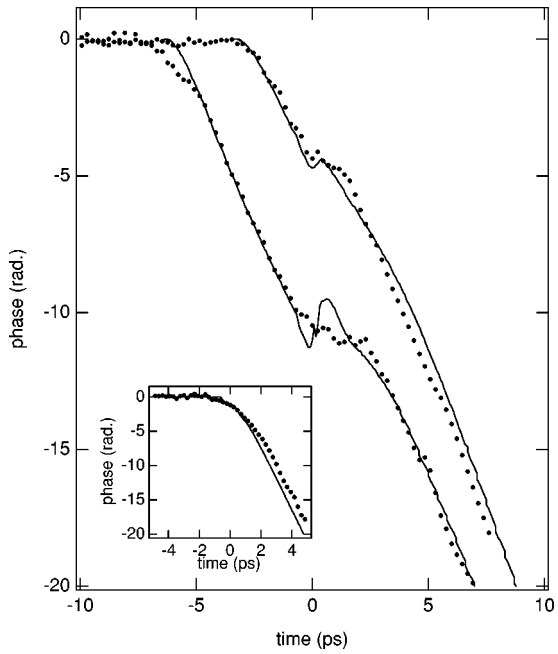

FIG. 3. Phase shift of *S*-polarized probe beam as a function of time following the interaction of a pure carbon target with the 400 fs duration LULI laser pulse and prepulse. Experiment (circles) and FILM simulations (solid line) are compared for a prepulse delay of 3 ps (upper curve, laser intensities of 5×10^{14} and 2.5×10^{17} W/cm^2 for the prepulse and the main pulse, respectively) and 6 ps (lower curve, laser intensities of 1×10^{15} and 5×10^{17} W/cm^2). The insert shows the phase shift of the *S*-polarized probe beam as a function of time for the main pulse alone, at an intensity of 2.5×10^{17} W/cm^2. The peak of the main pulse is at zero time for all the plots.

evaluate laser absorption by solving the Maxwell equations in a steep gradient plasma. The ponderomotive force was calculated from first principles, i.e., the gradient of the field energy density inside the plasma. The phase shift experienced by the probe beam was postprocessed from the FILM results using the same electromagnetic solver. The agreement shown in Fig. 2 is typical: the noise in the phase data governs the uncertainty in the laser irradiance used in the simulation. Experimental irradiance uncertainties are larger than 50% owing to the difficulty to measure the laser energy and focal spot size for frequency-doubled laser light. Because the hydrocode and experimental results agree quite well, we note that the electron density gradient scale length can be determined directly from the code with high accuracy. Results for the 3 ps and the 6 ps delays are $L/\lambda=0.16\pm0.01$ and $L/\lambda=0.71\pm0.01$, respectively. This confirms the values obtained from the (*P*-*S*) phase difference measurements.

Figure 3 shows the phase shift of the *S*-polarized probe beam when both the prepulse and the main pulse are interacting with the target. FILM simulation results are superimposed. Only the region corresponding to the center of the main pulse focal spot is shown. A strong, quasispectrally continuous emission is observed in the probe beam direction when the probe and the ''pump'' beams are overlapped in time. This spurious effect is exploited to determine experimentally the time of the peak of the laser pulse by using the

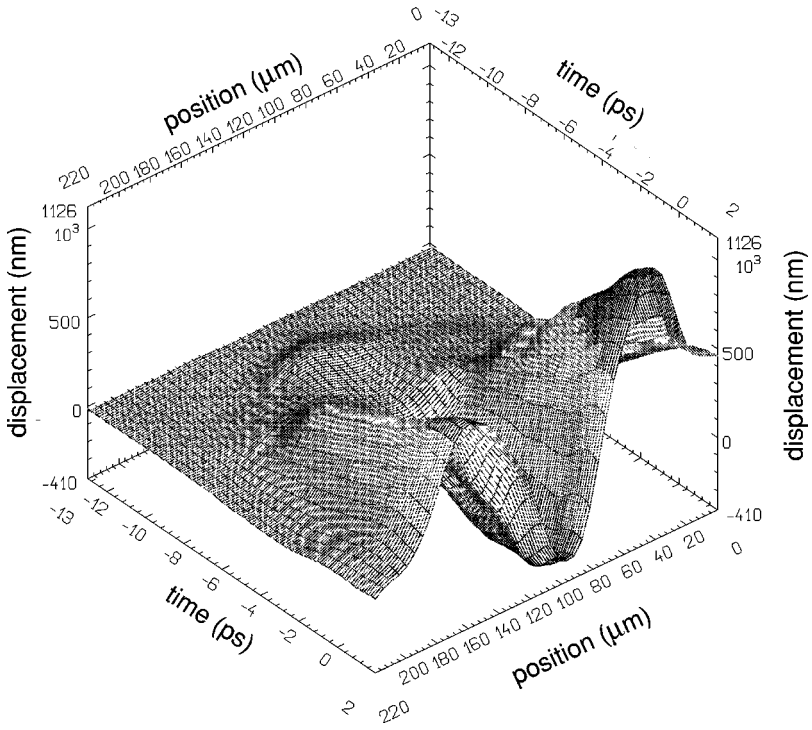

FIG. 4. Absolute position of the *S*-polarized probe beam turning point as a function of space and time following the interaction of a pure carbon target with the 400 fs duration LULI laser pulse and prepulse. The spatial axis is along a line passing by the center of the focal spot. Time zero is the peak of the main pulse. Negative coordinates correspond to a motion towards the target. The spatiotemporal phase shift produced by the prepulse has been subtracted.

fact that the continuum radiation and the probe beams interact coherently over the region near zero time delay [32]. In Fig. 3, the important point is that our measurement technique follows the absolute position of the probe beam turning point. We clearly see that the interaction with the main pulse almost stops the plasma expansion. For a 3 ps prepulse delay, the density gradient is still rather steep and the effect is small. The physical reason for the small influence of the rather large ponderomotive pressure in steep gradients is simply that the hydrodynamic scale length is much less than the laser wavelength. The inset in Fig. 3 shows the phase shift measured without the prepulse, as a function of time. One can clearly appreciate the role of the finite prepulse-induced scale length on the plasma expansion velocity by noting that the absolute phase shift at 4 ps after the laser peak is only half its value when the prepulse is applied. We also note a slight discrepancy between the hydrocode results and the experiment, in the shape of the temporal variation of the phase around the peak of the main pulse, when the ponderomotive force have its maximum effect on the plasma electron density gradient. For a 6 ps prepulse delay, the electron density gradient scale length is larger and the laser ponderomotive force effects are even more pronounced. FILM predictions exhibit a jagged shape that we attribute to a poor fluid description of the ion response to the laser pressure. However, we note that in agreement with previous laser absorption measurements performed in the same irradiance and pulse duration range [33], our simulations correctly predict a reduced absorption for higher laser intensities. This effect contributes, in addition to the increased impact of the laser pressure for longer gradient scale lengths, to the lower expansion velocity noticed at 5 ps after the main pulse in the 6 ps delay case, as compared to the 3 ps delay case. In the 6 ps delay case, we also want to point out that the onset of the critical surface motion is slightly perturbed, as compared to the lower energy, 3 ps case. We attribute this effect to poorly controlled spectral phase perturbations during amplification, which are not compensated for during recompression, at higher laser energies.

Figure 4 shows the absolute position of the probe beam turning point (electron density of 8×10^{20} cm^{-3}) as a function of space along a diameter of the main pulse focal spot and as a function of time. The time scale origin corresponds to the peak of the laser pulse. The center of the focal spot is located at 100 μm. In analyzing these results, it is very important to remember that the motion of the turning point due to the prepulse (6 ps delay) has been subtracted. Because of the nonuniform laser intensity distribution in the focal spot, the residual laser energy, in a 120 μm diameter around the focal spot center, produces an increase of the expansion motion towards the laser. This explains the double bump feature at ±50 μm from the focus center. As noted before, most of the laser energy is located near the center of the focal spot (at 100 μm in Fig. 4). There, the probe beam turning point motion is clearly towards the target (negative coordinates). This is a direct observation of the critical surface recess under the influence of the light pressure. Small ripples in the time range before -8 ps are related to an imperfect subtraction of the measured phase shift from two different shots, i.e., one with the prepulse alone and the other with both pulses.

In conclusion, we have implemented a new design for single-shot frequency-domain interferometry that enables us to observe, with unprecedented time and space resolution, the effect of the laser ponderomotive force on a fully characterized plasma of varying electron density gradient scale length. The important point is that our measurement gives a direct mapping of the position of the critical density surface (related to the probe beam turning point). This is different

from velocity measurements obtained from Doppler shifts. After all, our results show relatively small perturbations of the critical surface velocity for steep electron density gradients, i.e., for no prepulse or for a 3 ps delay. This is in agreement with numerical simulations. Accordingly, we have some difficulties in reconciling our results with those of Ref. [7] that were obtained at the same wavelength ($0.529\ \mu$m), probably a similar intensity contrast ratio, the same pulse duration, but ten times lower laser irradiances. To extrapolate the present work to higher irradiances would need to master optical techniques in an environment of highly nonlinear media and wave-mixing perturbations between the laser-producing and the probe beams and to abandon fluid simulations for kinetic models in the interpretation of the data.

We gratefully acknowledge the support of the LULI laser staff and illuminating discussions with Arnold Migus and Patrick Mora.

[1] G. Mourou *et al.*, Phys. Today **51**(1), 22 (1998).
[2] H.M. Milchberg *et al.*, Phys. Plasmas **3**, 2149 (1996).
[3] T.R. Clark *et al.*, Phys. Rev. E **61**, 1954 (2000).
[4] E. Esarey *et al.*, IEEE J. Quantum Electron. **33**, 1879 (1997), and references therein.
[5] R. Kodama *et al.*, Phys. Rev. Lett. **77**, 4906 (1996).
[6] K.A. Tanaka *et al.*, Phys. Plasmas **7**, 2014 (2000), and references therein.
[7] X. Liu and D. Umstadter, Phys. Rev. Lett. **69**, 1935 (1992).
[8] C.Y. Chien *et al.*, Opt. Lett. **18**, 1535 (1993).
[9] O. Peyrusse *et al.*, Phys. Rev. Lett. **75**, 3862 (1995).
[10] S.C. Wilks *et al.*, Phys. Rev. Lett. **69**, 1383 (1992); S.C. Wilks, Phys. Fluids B **5**, 2603 (1993).
[11] E.G. Gamaly, Phys. Rev. E **48**, 2924 (1993).
[12] O.L. Landen *et al.*, Phys. Rev. Lett. **63**, 1475 (1989).
[13] T. Dewandre, J.R. Albritton, and E.A. Williams, Phys. Fluids **24**, 528 (1981).
[14] O.L. Landen, D.G. Stearns, and E.M. Campbell, Phys. Rev. Lett. **63**, 1475 (1992).
[15] M.P. Kalashnikov *et al.*, Phys. Rev. Lett. **73**, 260 (1994).
[16] R. Sauerbrey, Phys. Plasmas **3**, 4712 (1996).
[17] M. Zepf *et al.*, Phys. Plasmas **3**, 3242 (1996).
[18] H.M. Milchberg and R.R. Freeman, Phys. Rev. A **41**, 2211 (1990).
[19] J.-P. Geindre *et al.*, Opt. Lett. **19**, 1997 (1994).
[20] N. Scherer *et al.*, J. Chem. Phys. **95**, 1487 (1991).
[21] P. Audebert *et al.*, Phys. Rev. Lett. **73**, 1990 (1994).
[22] J.-R. Marquès *et al.*, Phys. Rev. Lett. **76**, 3566 (1996).
[23] R. Evans *et al.*, Phys. Rev. Lett. **77**, 3359 (1996).
[24] P. Blanc *et al.*, J. Opt. Soc. Am. **13**, 118 (1996).
[25] C. Quoix *et al.*, Eur. Phys. J.: Appl. Phys. **5**, 163 (1999).
[26] C. Quoix *et al.*, J. Quant. Spectrosc. Radiat. Transf. **65**, 455 (2000).
[27] A. Benuzzi-Mounaix *et al.*, Phys. Rev. E **60**, R2488 (1999).
[28] S. Rebibo *et al.*, Laser Part. Beams **19**, 67 (2001).
[29] E.G. Gamaly, Phys. Fluids B **5**, 3765 (1993).
[30] X. Liu *et al.*, Opt. Lett. **20**, 1163 (1995).
[31] U. Teubner *et al.*, Phys. Plasmas **3**, 2679 (1996).
[32] E.P. Ippen and C.V. Shank, in *Ultrashort Light Pulses, Picosecond Techniques and Applications*, edited by L. Shapiro (Springer, Berlin, 1977), pp. 83–122.
[33] D.F. Price *et al.*, Phys. Rev. Lett. **75**, 252 (1995).